Supplementary Materials for PEA_2PbI_4: Fast Two-Dimensional Lead Iodide Perovskite Scintillator with Green and Red Emission

Dominik Kowal[a], Michal Makowski[b], Marcin Eugeniusz Witkowski[b], Roberto Cala'[c,d], Md Abdul Kuddus Sheikh[a], Muhammad Haris Mahyuddin[e], Etiennette Auffray[c], Winicjusz Drozdowski[b], Daniele Cortecchia[f,*], Muhammad Danang Birowosuto[a,*]

[a]*Łukasiewicz Research Network-PORT Polish Center for Technology Development, Stabłowicka 147, Wrocław, 54-066, Poland*
[b]*Institute of Physics, Faculty of Physics, Astronomy, and Informatics, Nicolaus Copernicus University in Torun, ul. Grudziadzka 5, Torun, 87-100, Poland*
[c]*CERN, Esplanade des Particules 1, Meyrin, 1211, Switzerland*
[d]*Università degli Studi di Milano-Bicocca, Piazza della Scienza 3, Milano, 20126, Italy*
[e]*Faculty of Mathematics and Natural Sciences, Institut Teknologi Bandung, Jl. Ganesha 10, Bandung, 40132, Indonesia*
[f]*Istituto Italiano di Tecnologia, Center for Nano Science and Technology (CNST@PoliMi), Via Pascoli 70, Milan, 20133, Italy*

Abstract

Fig. S1. Measured X-ray diffraction spectra with the respective theoretical diffractogram of PEA_2PbI_4.
Fig. S2. Absorption spectrum of PEA_2PbI_4 with Elliot fitting formalism.
Table S1. Lattice parameters from Reitveld refinement and bandgap from density functional theory (DFT) calculations and Elliot fits.
Fig. S3. Steady-state radioluminescence (RL) and afterglow fit at 10 K.
Fig. S4. The fit of glow curve with multiple Randal-Wilkins equation.
Fig. S5. Light yield stability for six hours in the standard atmosphere.
Fig. S6. Scintillation decay curve of single crystal in a 50-ns time window.
Table S2. Scintillation properties of PEA_2PbI_4 and other perovskite and BaF_2 scintillators.

*Corresponding author
Email addresses: daniele.cortecchia@iit.it (Daniele Cortecchia), muhammad.birowosuto@port.lukasiewicz.gov.pl (Muhammad Danang Birowosuto)

Fig. S7. RL spectra at 10 K and the photograph of PEA_2PbI_4 crystals synthesised with varying precursor concentrations.
Table S3. Light yields of PEA_2PbI_4 crystals derived from RL intensities.

---

1. X-ray diffraction, absorption spectra fitting, and crystal lattice parameters

The X-ray diffraction (XRD) spectrum in Figure S1 was analyzed the peaks and determined for the baseline. Then, using FullProf XRD software, we performed Rietveld refinement with the inputs from previous lattice parameters of [1]. The comparison of the parameters are shown in Table S1. The goodness of the refinement shown by χ^2 of 5.

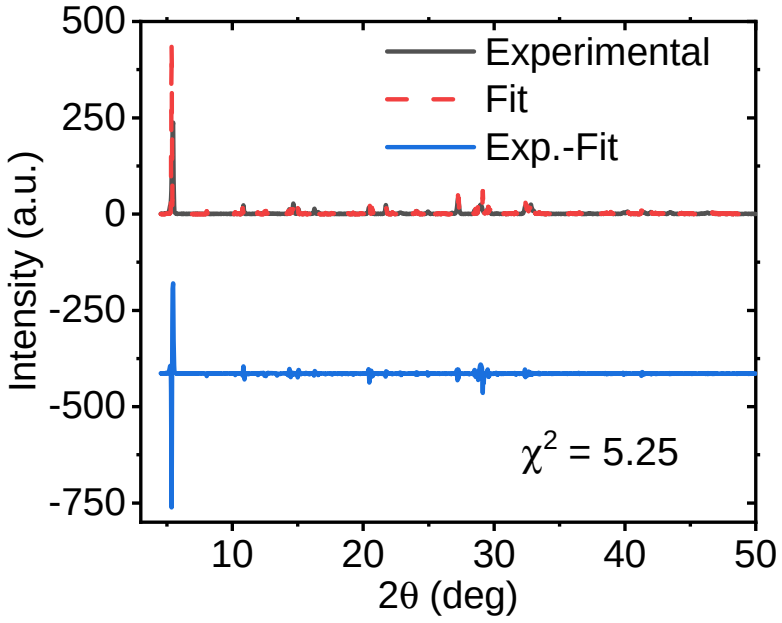

Figure S1: Measured XRD diffractogram for PEA_2PbI_4 single crystal with the respective theoretical fit and the difference between experiment and fit.

The fit to absorption spectrum in Figure S2 was performed by Elliot formalism [2]. In principle, the contributions to the absorption coefficient (α) can be defined from free carriers (continuum) (α_c) and excitons (α_{ex}).

$$\alpha(\hbar\omega) = \alpha_c + \alpha_{ex} \tag{S1}$$

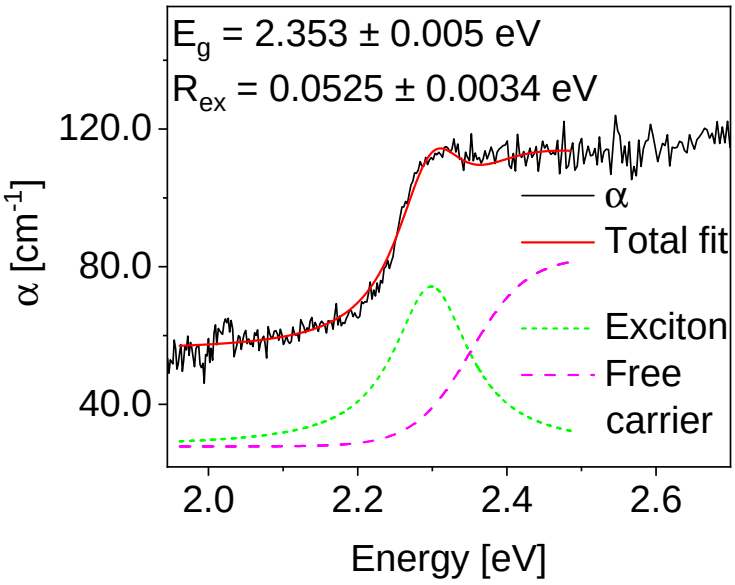

Figure S2: Absorption spectrum from PEA_2PbI_4 single crystal and their fitting contribution curves with Elliot method in Equations S1 and S2.

$$\alpha(\hbar\omega) = P_{cv}\left[\theta(\hbar\omega - E_g)\cdot\left(\frac{\pi e^{\pi x}}{\sinh(\pi x)}\right) + R_{ex}\sum_{n=1}^{\infty}\frac{4\pi}{n^3}\cdot\delta\left(\hbar\omega - E_g + \frac{R_{ex}}{n^2}\right)\right] \tag{S2}$$

where the frequency dependence of P_{cv} is approximated as a constant and related to the interband transition matrix element, $\hbar\omega$ is the photon energy, $\theta(\hbar\omega - E_g)$ is the heavyside step fuction, x is defined as $\sqrt{R_{ex}/(\hbar\omega - E_g)}$, and δ denotes a delta function, R_{ex} is exciton Rydberg energy, n is the principle quantum number. From the fits, we obtained E_g^{abs} of 2.353 $\pm$ 0.005 eV.

Table S1: Summary of the crystal data, structure refinements, and bandgaps (density functional theory (DFT) calculation (E_{gap}^{DFT}) and absorption spectra (E_{gap}^{abs})) for PEA_2PbI_4 from our works and Reference [1, 3].

Compound name	PEA_2PbI_4 (our works)	PEA_2PbI_4[1, 3]
Empirical formula	$(C_6H_5(CH_2)_2NH_3)_2PbI_4$	
Formula weight	959.17	
Crystal system	Triclinic	
Space group	$P\bar{1}$	
Temperature (K)	296	
λ (Å)	0.7107	
a (Å)	8.5835(2)	8.7389(2)
b (Å)	8.6833(2)	8.7403(2)
c (Å)	33.2053(4)	32.9952(6)
α (°)	85.151(1)	84.646(1)
β (°)	85.128(1)	84.657(1)
γ (°)	90.392(1)	89.643(1)
V (Å^3)	2456.88(5)	2498.29(9)
Z	4	
ρ (g/cm^3)	2.593	2.550
E_{gap}^{DFT} (eV)	2.134	2.060
E_{gap}^{abs} (eV)	2.249	2.580

2. Steady-state XL, afterglow and thermoluminescence

From the fit of the afterglow with three exponential decay components as shown in Figure S3, we obtain the components of 5, 33, and 364 s with contributions of 10, 32, and 58 %, respectively. The components are still much slower than those of 10 and 80 s of 83 and 17 % from PEA_2PbBr_4 [4].

For the quantitative analysis of the glow curve in Figure S4, we deconvolute it into 3 glow peaks using the classic Randall-Wilkins equations[5, 6]:

$$I_{TL} = \sum_{i=1}^{k=3} n_{0_i} V \sigma_i \exp\left(-\frac{E_i}{k_B T}\right) \exp\left(-\frac{\sigma_i}{\beta}\int_{T_0}^{T} \exp\left(-\frac{E_i}{k_B T'}\right) dT'\right) \quad \text{(S3)}$$

where T is the temperature, β is the heating rate, k_B is the Boltzmann constant, n_{0_i} is the initial trap concentration, V is the crystal volume, E_i

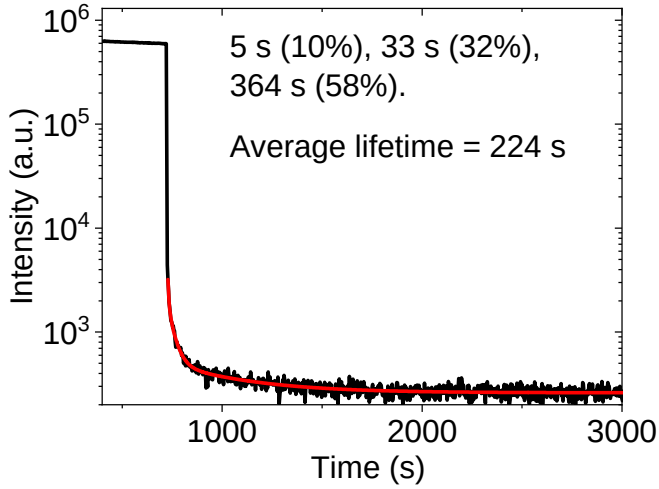

Figure S3: Steady-state RL and afterglow at 10 K of PEA_2PbI_4 single crystal with its fit. Afterglow parts were recorded after 10 minutes of X-ray irradiation at 10 K.

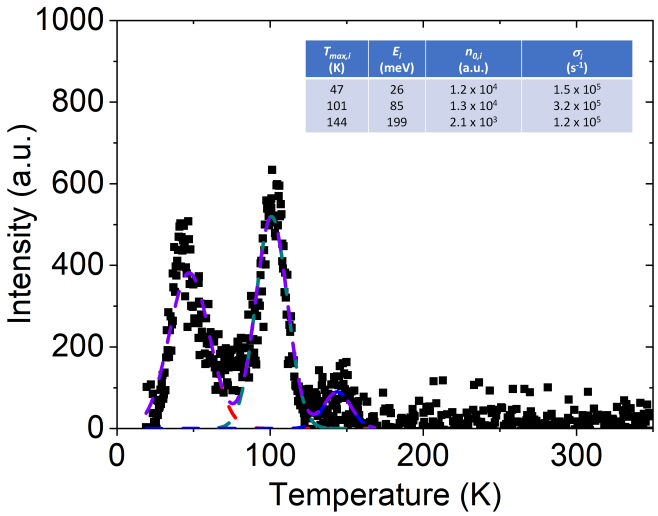

$T_{max,i}$ (K)	E_i (meV)	$n_{0,i}$ (a.u.)	σ_i (s^{-1})
47	26	1.2×10^4	1.5×10^5
101	85	1.3×10^4	3.2×10^5
144	199	2.1×10^3	1.2×10^5

Figure S4: The fit of glow curve of PEA_2PbI_4 single crystal with multiple Randal-Wilkins equations[5, 6]. The parameters of the fit are shown in the inset.

is the trap depth, and σ_i is the frequency factor of each component. The unit-less $n_{0_i}V$ or A_i in Figure S4 is used to compare afterglow of different crystals. Although A_i values of $\sim 10^4$ are still comparable with those of

PEA_2PbBr_4, the E_i depths between 26 and 199 meV are much deeper than that of 10 meV from PEA_2PbBr_4 [4, 7].

3. Light yield stability as a function of time

To test the stability of the light yield of PEA_2PbI_4 to the ambient environment, we measured the pulse height spectra of the samples for 6 hours and the derived values of the light yield were plotted with the normalized values at the initial time as shown in Figure S5.

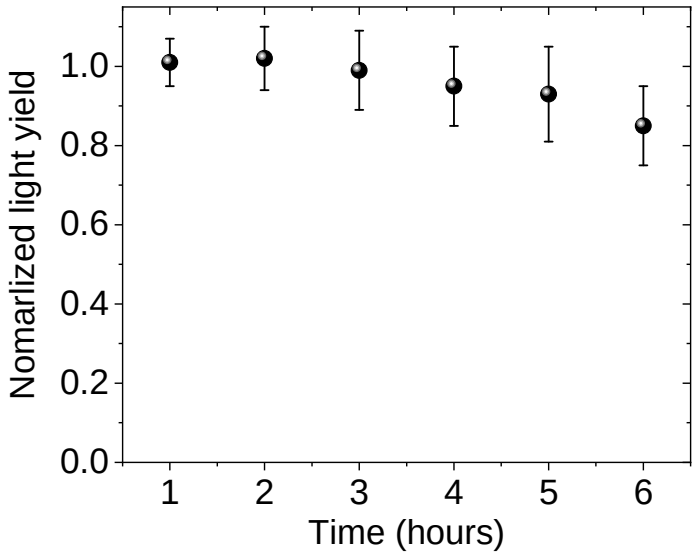

Figure S5: Normalized light yield vs. time of PEA_2PbI_4 single crystal while exposed to environmental conditions (standard atmosphere, 65% humidity).

4. Short-time-scale scintillation decay curve

In order to resolve the fastest short components of decay curve, we measured the scintillation decay curve in the time scale of 50 ns. Using the components and contributions from the curve in Fig. S6, we reconstruct the total components and contributions in long-time-scale decay curve shown in Fig. 3b.

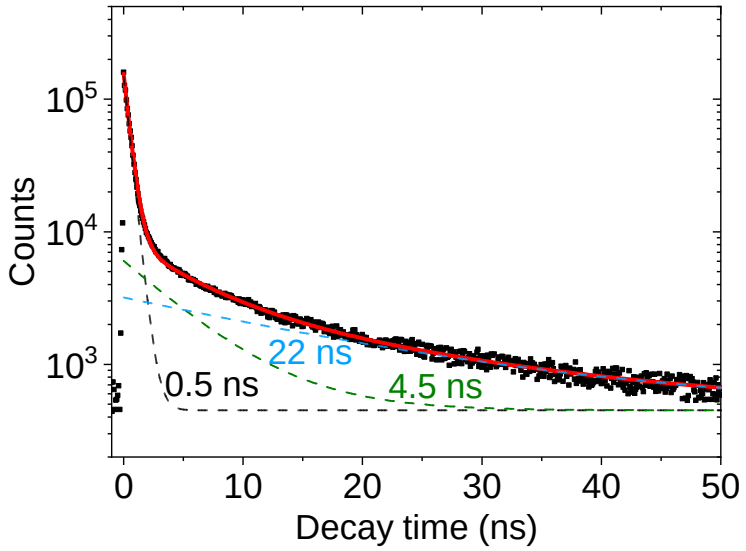

Figure S6: The scintillation decay curve of PEA_2PbI_4 single crystal shown in the semi-logaritmic scale over a range of 50 ns. Three-exponential fit with the components are shown as solid and dashed lines, respectively.

5. Comparison of scintillation performance of the reported PEA_2PbI_4, some other 2D HOIP scintillators and commercial scintillator BaF_2

Table S2: Comparison of scintillation properties of PEA_2PbI_4 with the literature data for some other 2D HOIP and BaF_2 scintillators. The parameters are mass density ρ, absorption length at 50 keV ℓ_{50keV}, light yield at room temperature LY, energy resolution E_{res}, central wavelength of the emission band λ and fastest decay time constant τ_{fast} with their contribution to the total light yield C.

Scintillator	ρ [g/cm^3]	ℓ_{50keV} [mm]	LY [ph/MeV]	E_{res} [%]	λ [nm]	$\tau_{fast}(C)$ [ns (%)]	Ref.
PEA_2PbI_4	2.59	0.5	1,000	35	660	0.5 (10)	Current
PEA_2PbBr_4	2.36	1.1	11,000	11.2	414	13.4 (94.9)	[4, 7]
CHA_2PbBr_4	2.38	1.1	4,500	-	420	0.4 (4)	[8]
$(EDBE)PbBr_4$	2.88	0.8	10,000	-	520	1.1 (5)	[8]
$(API)PbBr_4$	3.03	0.9	3,500	-	422	1.4 (6)	[8]
OA_2PbI_4	2.21	0.6	100	-	520	0.3 (49)	[8]
BaF_2	4.88	0.2	10,000	10	220	0.8 (14)	[9, 10]

In Supplementary Table S2, some of the most important scintillation properties of PEA_2PbI_4, PEA_2PbBr_4 ,CHA_2PbBr_4, (EDBE)$PbBr_4$, (API)$PbBr_4$, OA_2PbI_4 and BaF_2 are summarized. The bromide scintillators still have the largest light yields for 2D HOIP, but for the absorption lengths are much longer than iodide ones. Comparing to the last 2D HOIP iodide scintillators [8], the light yields PEA_2PbI_4 of 1,000 ph/MeV is already ten times than before. In addition, the fast decay time is still comparable with BaF_2.

6. Comparison of the scintillation performance of PEA_2PbI_4 crystals grown with varying concentration and synthesis method

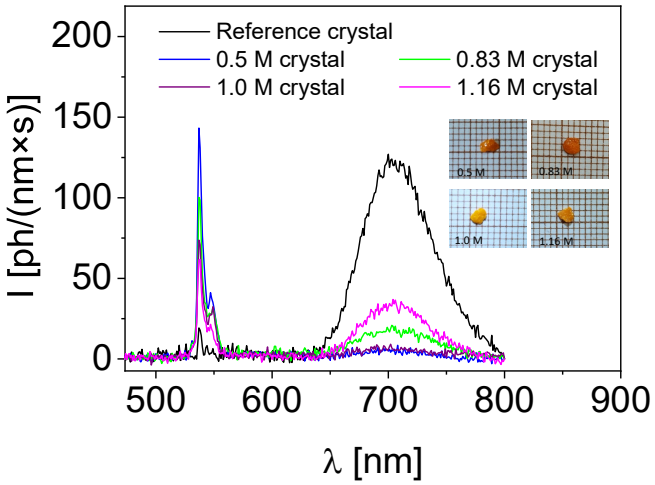

Figure S7: RL spectra taken at 10K for the PEA_2PbI_4 crystals grown with varying concentration and the reference (optimized) PEA_2PbI_4 sample. The inset presents photographs of the PEA_2PbI_4 samples for varying concentration.

Table S3: Light yield LY in [ph/MeV] of the PEA_2PbI_4 crystal samples grown with varying concentration compared to reference sample from main manuscript

T	LY [ph/MeV]				
	Reference sample	0.5 M	0.83 M	1.0 M	1.16 M
10K	10,000	2000	3,000	1980	3450
300K	1,000	<100	<100	<100	<100

PEA_2PbI_4 crystals have been synthesised with varying molar concentration of the precursors. The synthesis method has been slightly modified in respect to the one reported in the Experimental Section of the manuscript. Hydroiodic acid (HI, 57% w/w acqueous solution), phenethylammonium iodide ((PEA)I, 98%), and lead iodide (PbI_2, 98%) were purchased from Sigma-Aldrich. The precursor solutions were prepared by dissolving equal molar amount of (PEA)I and PbI_2 in HI under stirring at 100 °C for 30 minutes. Various concentration of 0.5 M, 0.83 M, 1.0 M, and 1.16 M. The crystals precipitated were then collected by filtration and dried overnight at 40 °C under vacuum. Those crystals are much faster in fabrication than PEA_2PbI_4 crystal in the main manuscript. Finally, the perovskite was then stored in glove box under nitrogen before further characterization. Fig. S7 presents the RL spectra of the examined PEA_2PbI_4 samples as compared to the reference sample RL spectrum (for higher signal to noise ratio, the figure presents comparison of spectra taken at 10 K). Photographs of the new PEA_2PbI_4 samples are showed in the inset of the figure. The RL signal consists of the same narrowband green and broadband red emission as for the reference sample, but the contribution of the both is varied. The overall LY data at 10K and RT are gathered at Table S3. Among the new crystals, one that was grown with highest molar concentration (1.16 M) gives the highest number of overall LY at 10K, however it still does not reach the LY number obtained for the reference sample. At RT, the RL of the new PEA_2PbI_4 samples is quenched, resulting in small number of LY which is below 100 ph/MeV. It seems that there is a trade-off among the fabrication time, quality, and scintillation properties of PEA_2PbI_4 crystals.

References

[1] K.-z. Du, Q. Tu, X. Zhang, Q. Han, J. Liu, S. Zauscher, D. B. Mitzi, Two-dimensional lead(ii) halide-based hybrid perovskites templated by acene alkylamines: Crystal structures, optical properties, and piezoelectricity, Inorg. Chem. 56 (15) (2017) 9291–9302.

[2] R. J. Elliott, Theory of the effect of spin-orbit coupling on magnetic resonance in some semiconductors, Phys. Rev. 96 (1954) 266–279.

[3] B. Febriansyah, T. M. Koh, Y. Lekina, N. F. Jamaludin, A. Bruno, R. Ganguly, Z. X. Shen, S. G. Mhaisalkar, J. England, Improved photovoltaic efficiency and amplified photocurrent generation in meso-

porous n = 1 two-dimensional lead–iodide perovskite solar cells, Chem. Mater. 31 (3) (2019) 890–898.

[4] F. Maddalena, A. Xie, Arramel, M. E. Witkowski, M. Makowski, B. Mahler, W. Drozdowski, T. Mariyappan, S. V. Springham, P. Coquet, C. Dujardin, M. D. Birowosuto, C. Dang, Effect of commensurate lithium doping on the scintillation of two-dimensional perovskite crystals, J. Mater. Chem. C 9 (2021) 2504–2512.

[5] M. D. Birowosuto, D. Cortecchia, W. Drozdowski, K. Brylew, W. Lachmanski, A. Bruno, C. Soci, X-ray scintillation in lead halide perovskite crystals, Sci. Rep. 6 (2016) 37254.

[6] J. T. Randall, M. H. F. Wilkins, Phosphorescence and electron traps. i. the study of trap distributions, Proc. R. Soc. Lond. A 184 (999) (1945) 365–389.

[7] A. Xie, C. Hettiarachchi, F. Maddalena, M. E. Witkowski, M. Makowski, W. Drozdowski, Arramel, A. T. S. Wee, S. V. Springham, P. Q. Vuong, H. J. Kim, C. Dujardin, P. Coquet, M. D. Birowosuto, C. Dang, Lithium-doped two-dimensional perovskite scintillator for wide-range radiation detection, Comms. Mater. 1 (2020) 37.

[8] A. Xie, F. Maddalena, M. E. Witkowski, M. Makowski, B. Mahler, W. Drozdowski, S. V. Springham, P. Coquet, C. Dujardin, M. D. Birowosuto, C. Dang, Library of two-dimensional hybrid lead halide perovskite scintillator crystals, Chem. Mater. 32 (19) (2020) 8530–8539.

[9] M. Laval, M. Moszyński, R. Allemand, E. Cormoreche, P. Guinet, R. Odru, J. Vacher, Barium fluoride — inorganic scintillator for subnanosecond timing, Nuclear Instruments and Methods in Physics Research 206 (1) (1983) 169–176.

[10] R. H. Pots, E. Auffray, S. Gundacker, Exploiting cross-luminescence in baf_2 for ultrafast timing applications using deep-ultraviolet sensitive hpk silicon photomultipliers, Front. Phys. 8 (2020) 592875.